

SOFT DIPOLE MODE IN ${}^8\text{He}$

L. V. Grigorenko^{a,b,c}, *M. S. Golovkov*^a, *G. M. Ter-Akopian*^a,
A. S. Fomichev^a, *Yu. Ts. Oganessian*^a, *V. A. Gorshkov*^a,
S. A. Krupko^a, *A. M. Rodin*^a, *S. I. Sidorchuk*^a,
R. S. Slepnev^a, *S. V. Stepantsov*^a, *R. Wolski*^{a,d},
D. Y. Pang^{a,e}, *V. Chudoba*^{a,f}, *A. A. Korshennikov*^c,
E. A. Kuzmin^c, *E. Yu. Nikolskii*^c, *B. G. Novatskii*^c,
D. N. Stepanov^c, *P. Roussel-Chomaz*^g, *W. Mittig*^g, *A. Ninane*^h,
*F. Hanappe*ⁱ, *L. Stuttgé*^j, *A. A. Yukhimchuk*^k, *V. V. Perevozchikov*^k,
Yu. I. Vinogradov^k, *S. K. Grishechkin*^k, *S. V. Zlatoustovskiy*^k

^a Joint Institute for Nuclear Research, Dubna

^b Gesellschaft für Schwerionenforschung mbH, Darmstadt, Germany

^c RRC «The Kurchatov Institute», Moscow

^d Henryk Niewodniczanski Institute of Nuclear Physics, Cracow, Poland

^e Department of Technical Physics, Peking University, Beijing, China

^f Faculty of Philosophy and Science, Silesian University in Opava, Opava, Czech Republic

^g GANIL, Caen Cedex 5, France

^h Slashdev Integrated Systems Solutions Rue de la Rochette, Gembloux, Belgium

ⁱ Université Libre de Bruxelles, PNTPM, Bruxelles, Belgium

^j Institut de Recherches Subatomiques, IN2P3/Université Louis Pasteur, Strasbourg, France

^k RFNC — All-Russian Scientific Research Institute of Experimental Physics, Sarov, Russia

The low-lying spectrum of ${}^8\text{He}$ was studied in the ${}^3\text{H}({}^6\text{He}, p){}^8\text{He}$ transfer reaction for small center of mass angles. The 0^+ ground state (g.s.) of ${}^8\text{He}$ and excited states, 2^+ at 3.6–3.9 MeV and (1^+) at 5.3–5.5 MeV, were populated with cross sections of 200, 100–250, and 90–125 $\mu\text{b}/\text{sr}$. Some evidence for the excited state at about 7.5 MeV can be found in the data. The possible nature of the near-threshold anomaly above 2.14 MeV in ${}^8\text{He}$ is related to the population of a 1^- continuum (soft dipole excitation) with a peak energy value at about 3 MeV. This assumption can probably resolve the problem of a large uncertainty existing in the experimental data on the ${}^8\text{He}$ 2^+ state energy.

Спектр ${}^8\text{He}$ был изучен в реакции передачи ${}^3\text{H}({}^6\text{He}, p){}^8\text{He}$ для маленьких углов в системе центра масс. В ${}^8\text{He}$ были заселены основное состояние 0^+ , а также его возбужденные состояния 2^+ при 3,6–3,9 МэВ и (1^+) при 5,3–5,5 МэВ с сечениями 200, 100–250 и 90–125 мкб/ср соответственно. В измеренном спектре ${}^8\text{He}$ также имеется указание на возбужденное состояние, находящееся при энергии около 7,5 МэВ. Аномалия, обнаруженная в спектре ${}^8\text{He}$ непосредственно над порогом развала на ${}^6\text{He} + 2n$ при энергии 2,14 МэВ, может быть вызвана заселением континуума 1^- («мягкое» дипольное возбуждение) с величиной энергии пика около 3 МэВ. Это предположение, вероятно, сможет разрешить проблему большой неопределенности, имеющейся в экспериментальных данных различных авторов для энергии состояния 2^+ в ${}^8\text{He}$.

PACS: 25.60.Je; 21.60.Gx

INTRODUCTION

Since the discovery of the ^8He isotope in the early 60s a lot of efforts were invested in its study. Literature on ^8He exceeds *two hundred* titles (e.g., [1]). This interest is understandable. From nuclear structure point of view ^8He is a very well clusterized system; it is considered to be a perfect example of four-neutron halo. As one of the lightest dripline nuclei it has always been an important «playground» for testing theoretical models. However, if one looks through the standard compilation [2], one finds that the first 2^+ excited state of ^8He is defined with a large uncertainty $E^* = 2.7\text{--}3.6$ MeV (in this paper E^* denotes the excitation energy of ^8He and E stands for the ^8He energy relative to the $^6\text{He} + n + n$ breakup threshold). Such a large uncertainty is unsatisfactory as the positions of the first 2^+ states in the even nuclei are very well understood theoretically and typically reliably related to other observables (deformations, $B(E2)$ strengths, etc.). Therefore, the large uncertainty for the 2^+ state position imposes serious limitations on the precision of the related theoretical studies.

We have possibly found an explanation for the puzzle of the 2^+ state in ^8He . Our conclusions are based on the recent studies of the $^3\text{H}(^6\text{He}, p)^8\text{He}$ transfer reaction at the Flerov Laboratory of Nuclear Reactions (JINR, Dubna) [3] and a series of theoretical estimates. We demonstrate that it is very probable that the 2^+ state is typically observed in a mixture with a soft dipole mode (population of 1^- continuum) therefore providing confusing experimental signals.

The so-called soft mode of the giant dipole resonance is expected to be a common feature of the halo nuclei. This feature is related to the low binding energy of the halo neutrons which allows them low-frequency oscillations against the core creating low-lying dipole excitations. Experiments with ^{11}Li [4–6] and the other «classical» halo nuclei ^6He [7] and ^{11}Be [8] showed that the observed low-lying $E1$ strength is in good agreement with the cluster non-energy-weighted (NEW) sum rule (see, e.g., [9]). Theoretically, the soft $E1$ mode in the light neutron rich nuclei seems to be reasonably well understood on the basis of cluster models (e.g., [10, 11]). According to our estimates of this kind, one could expect the peak in the 1^- spectrum of ^8He at a *lower* than the 2^+ state energy, $E^* \sim 3$ MeV (the ^8He level scheme is shown in Fig. 1, *a*). Common wisdom about the soft dipole mode (e.g., [10–13]) is that the exact profile of the $E1$ spectrum populated in nuclear reactions should significantly depend on the details of the reaction mechanism. Therefore, it is possible that the interpretations of the entangled 2^+ and 1^- continuum spectra become confusing in some cases. The unit system $\hbar = c = 1$ is used in the part of this work where theory analysis is presented.

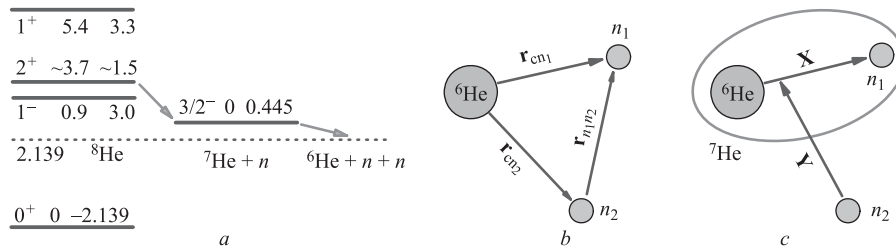


Fig. 1. *a*) Level scheme for ^8He and ^7He nuclei. Notation $\{J^\pi, E^*, E\}$ is used for the energy levels. The sequential decay path for ^8He 2^+ state is shown by arrows. Panels *b* and *c* show the coordinate set used in this work

1. EXPERIMENTAL SETUP

Experiment was performed at the JINR U400M cyclotron. A 34 MeV/amu beam of ${}^{11}\text{B}$ ions bombarded a 1 mm thick beryllium production target. The secondary ${}^6\text{He}$ nuclei escaping from the target at close to zero angles were separated from the other reaction products by the separator ACCULINNA [14] and focused in a 20 mm spot on the target cell filled with tritium gas to 900 mPa and cooled down to 28 K. The tritium target had twin entrance and exit windows sealed with 12.7 μm stainless steel foils. With a 4 mm layer of gas crossed by the ${}^6\text{He}$ projectile nuclei the thickness of the tritium target was $2.0 \cdot 10^{20} \text{ cm}^{-2}$. Typical beam intensity incident on the target was $\sim 4 \cdot 10^4 \text{ s}^{-1}$. The admixtures of other particles in the beam were no more than 7% and the beam diagnostics completely eliminated them.

Experimental setup and diagram elucidating the reaction kinematics are shown in Fig. 2. For small angles in the centre-of-mass system (cms), where maximal cross sections are expected for the ${}^3\text{H}({}^6\text{He}, p){}^8\text{He}$ reaction, the recoil protons fly back from the target in the lab. system. The residuals (${}^8\text{He}$) and their decay products (${}^6\text{He}$ and neutrons) are moving in a quite narrow angular cone in forward direction. A telescope consisting of one 300 μm and one 1 mm thick annular Si detectors met the recoil protons escaping back. The active areas of these detectors had the outer and inner diameters of 82 and 32 mm, respectively. The first detector was segmented in 16 rings on one side and 16 sectors on the other side and the second, 1 mm detector, was not segmented. This telescope was installed 100 mm upstream of the target and covered an angular range of $171\text{--}159^\circ$ in lab. system. A veto detector was installed upstream of the proton telescope to alert to the signals generated by the beam halo.

Zero angle telescope destined for the residual nuclei (${}^8\text{He}$, ${}^6\text{He}$) was installed on the beam axis at a distance of 36.5 cm. This telescope was composed of six squared ($60 \times 60 \text{ mm}$) 1 mm thick Si detectors. The first two detectors of the telescope were segmented in 16 strips each in vertical and horizontal directions. All other detectors in the telescope were segmented in 16 strips.

A set of beam detectors was installed upstream of the veto detector (not shown in Fig. 2). Two 0.5 mm plastic scintillators placed on a 8 m base provided the identification and energy measurement for projectile nuclei. Beam particles were readily recognized by comparing their flight times and energy losses in the plastics. Provided that the time-of-flight resolution was 0.5 ns, the overall resolution in the energy measurements done for individual beam nuclei

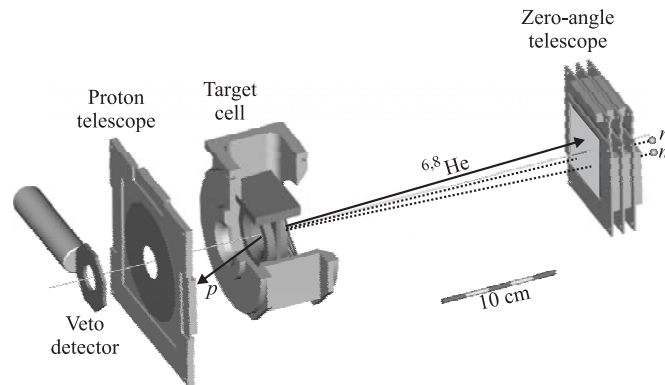


Fig. 2. Experimental setup and kinematical diagram

was better than 1% (FWHM). Two pairs of multiwire proportional counters installed 26 and 80 cm upstream of the target provided a 1.5 mm resolution for the hit positions of beam nuclei on the target.

Kinematical constraints, inherent to the ${}^3\text{H}({}^6\text{He}, p){}^8\text{He}$ reaction, allow only protons flying back from the target. For the proton telescope, the main background source was protons originating from the reactions in the target windows. Control irradiations performed with the empty target showed that this background was almost completely eliminated when p - ${}^8\text{He}$ or/and p - ${}^6\text{He}$ coincidences were considered. The detection of p - ${}^8\text{He}$ coincidence events granted selection for the reaction channel populating the ${}^8\text{He}$ g.s. For the decays of ${}^8\text{He}$ excited states the p - ${}^6\text{He}$ coincidences were selected to clean the missing mass spectrum and reconstruct the charged fragment energy in the cms of ${}^8\text{He}$.

Array of 48 detector modules of the neutron time-of-flight spectrometer DEMON [16] was installed in the forward direction at a distance of 3.1 m from the target. In more rare events where triple p - ${}^6\text{He}$ - n coincidences were detected the complete reaction kinematics was reconstructed.

The average ${}^6\text{He}$ projectile energy in the middle of the tritium target was about 25 MeV/amu; integral flux $2 \cdot 10^{10}$ was collected. The obtained missing mass spectrum of ${}^8\text{He}$ was measured up to 14 MeV. The upper limit was set by the proton detection threshold. Monte Carlo (MC) simulations taking into account the details of these experiments showed that a 450 keV (FWHM) resolution was inherent to the ${}^8\text{He}$ missing mass energy spectrum obtained from the data. The precision of the beam energy measurement was the critical point in the resolution achieved in this spectrum.

2. EXPERIMENTAL DATA

Two missing mass spectra of ${}^8\text{He}$ from the ${}^3\text{H}({}^6\text{He}, p){}^8\text{He}$ reaction are presented in Fig. 3. The ${}^8\text{He}$ spectrum obtained from the combination of the p - ${}^8\text{He}$ and p - ${}^6\text{He}$ coincidence data is shown in Fig. 3, *a*. The peak corresponding to the ${}^8\text{He}$ g.s. is well seen in the p - ${}^8\text{He}$ coincidence data. The tail visible on the right side of the g.s. peak was caused by the pile-ups in the second (non-segmented) detector of the proton telescope. Protons emitted from the target with energy ~ 8.5 MeV correspond to the g.s. peak of ${}^8\text{He}$. They passed through the $300 \mu\text{m}$ Si detector and were stopped in the second (1 mm) detector of the proton telescope. The background signals arose here from the beam halo particles (count rate of $(2 - 3) \cdot 10^3 \text{ s}^{-1}$). The veto detector allowed one to take away these events in the data analysis but the energy resolution of the second detector was deteriorated. As for the segmented $300 \mu\text{m}$ detector, the count rate per any of its sectors was at least 10 times lower. Consequently, the background signals did not damage the pulse height resolution. Protons with energy < 7.5 MeV were emitted from the target when excited states were populated in ${}^8\text{He}$ and practically all these protons were stopped in the $300 \mu\text{m}$ detector. Therefore, for the ${}^8\text{He}$ excited states the stated 450 keV resolution is valid.

Two peaks are well seen in the ${}^8\text{He}$ excitation spectrum. We can assign 2^+ to the ${}^8\text{He}$ resonance at excitation energy $E \approx 3.6$ MeV. The 2^+ resonance with energy (3.57 ± 0.12) MeV and width $\Gamma = (0.5 \pm 0.35)$ MeV was for the first time unambiguously and with a good precision, obtained in [15]. Later on, this resonance was reported in a number of papers with energy close to 3.6 MeV and width $\Gamma \approx 0.5 - 0.8$ MeV (see, e.g., [2, 17, and references

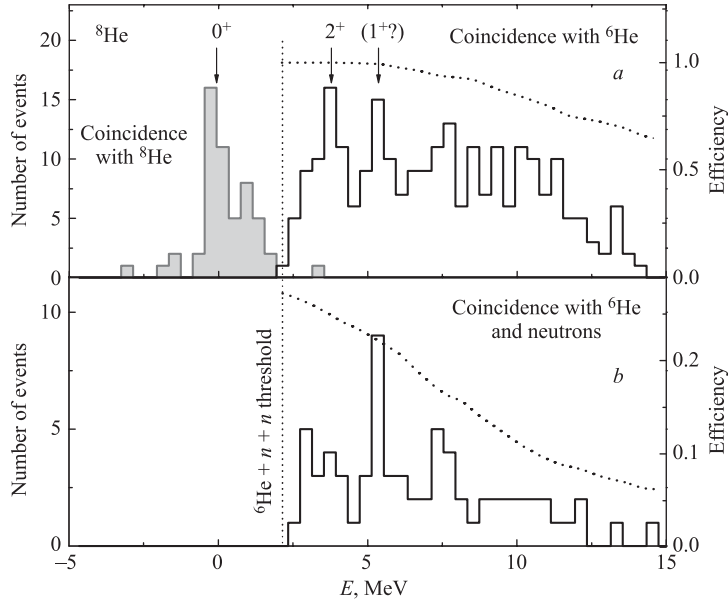


Fig. 3. Missing mass spectrum of ${}^8\text{He}$. *a*) The p - ${}^8\text{He}$ and p - ${}^6\text{He}$ coincidence data were used to obtain the ground state peak and the excited state spectrum, respectively. *b*) Spectrum built for the ${}^8\text{He}$ excited states from the p - ${}^6\text{He}$ - n coincidence data. The efficiencies of the p - ${}^6\text{He}$ and p - ${}^6\text{He}$ - n coincidence registrations are shown by dotted curves (see the right axes in both panels)

therein]). We assume that the $E \approx 5.4$ MeV peak seen in Fig. 3 is the 1^+ resonance of ${}^8\text{He}$. The ground for this assumption comes from various theoretical results (e.g., [21–23]) stably predicting that in the ${}^8\text{He}$ excitation spectrum the next state after the 2^+ should be the 1^+ state. We note that evidence for the peak at $E \sim 5$ – 6 MeV was found in [15]. The ${}^8\text{He}$ excited state at 5.4 MeV was recently reported also in [17]. Some evidence for the third excited state at about 7.5 MeV can be found in the spectra shown in Fig. 3.

A steep rise of the ${}^8\text{He}$ spectrum on the ${}^6\text{He} + n + n$ decay threshold is seen in Fig. 3. As we are going to demonstrate, this rise cannot be explained by the left «wing» of the 2^+ resonance. The possible explanation of the peculiar threshold behaviour of the ${}^8\text{He}$ spectrum is offered in Sec. 4.

Population cross section $\sim 200 \mu\text{b}/\text{sr}$ is found for the ${}^3\text{H}({}^6\text{He}, p){}^8\text{He}$ reaction populating the ${}^8\text{He}$ g.s. in a cms range of 4 – 10° . However, the observed threshold anomaly makes ambiguous and model-dependent the cross-section derivation for the excited states of ${}^8\text{He}$. The cross sections for the excited states are further discussed in Secs. 3 and 4.

3. WIDTH OF THE 2^+ STATE IN ${}^8\text{He}$

To interpret the data we need first to understand which cross-section behaviour we can expect above the ${}^6\text{He} + n + n$ threshold. The lowest known resonant state of ${}^8\text{He}$ is 2^+ at $E = 3.57$ MeV, $\Gamma = 0.5$ – 0.7 MeV. The inelastic cross-section profile for the 2^+ state can be

represented by the ordinary resonance expression

$$\sigma_{2^+}(E) \sim \frac{\Gamma_{2^+}(E)}{(E - E_{2^+})^2 + \Gamma_{2^+}^2(E)/4}. \quad (1)$$

The state decays sequentially via the ${}^7\text{He}$ ground state resonance ($3/2^-$ at $E_{3/2} = 0.445$ MeV, $\Gamma = 0.15$ MeV) by a p -wave neutron emission, see Fig. 1. The width for such decay can be given by a standard R -matrix expression

$$\Gamma_{l=1}(E) = \frac{2\gamma^2 P_{l=1}(E, r_{\text{ch}})}{1 + \gamma^2 (d/dE) S_{l=1}(E, r_{\text{ch}})} = \frac{\sqrt{8M} E^{3/2} (1 + 2EMr_{\text{ch}}^2) r_{\text{ch}} S_n}{(1 + 2EMr_{\text{ch}}^2)^2 + S_n}, \quad (2)$$

where M is the reduced mass for the channel and

$$\gamma = \frac{1}{2Mr^2} \theta^2 = \frac{1}{2Mr^2} S_n; \quad P_1(E, r) = \frac{\sqrt{8}(EM)^{3/2} r^3}{1 + 2EMr^2}; \quad S_1(E, r) = -\frac{1}{1 + 2EMr^2}. \quad (3)$$

Therefore, for the «two-body» estimate of the 2^+ state decay width via the $3/2^-$ g.s. in ${}^7\text{He}$ we can write

$$\Gamma_{2^+}^{(2b)}(E) = \Gamma_{l=1}(E - E_{3/2}). \quad (4)$$

This expression is valid only above the ${}^7\text{He} + n$ «threshold» and neglects the width of the unbound ${}^7\text{He}$ ground state.

A more accurate «three-body» expression can be used, which is valid in the whole energy range above the ${}^6\text{He} + n + n$ threshold:

$$\Gamma_{2^+}^{(3b)}(E) = S_{2n} \frac{(E - E_{xa} - E_{ya})^2 + \Gamma'^2/4}{2\pi} \int_0^E dE_x \frac{\Gamma_x(E_x)}{(E_x - E_{xa})^2 + \Gamma_x^2(E_x)/4} \times \frac{\Gamma_y(E - E_x)}{(E - E_x - E_{ya})^2 + \Gamma_y^2(E - E_x)/4}. \quad (5)$$

The resonance energies and width in our case are $E_{xa} = E_{ya} = E_{3/2}$, $\Gamma_x = \Gamma_y = \Gamma_{l=1}$. This equation is analogous to a quasiclassical expression for the three-body width obtained in [18, 19]. The latter was derived assuming $\Gamma^{(3b)}(E) \ll E$ and $E < E_x, E_y$. Consequently, it has unphysical peculiarity: it reduces to zero at $E = E_{xa} + E_{ya} = 2E_{3/2}$. Here, in Eq. (5), the factor in front of the integral is modified by $\Gamma'^2/4$ term. The value $\Gamma' = 0.31$ MeV is taken to get self-consistent result for width, namely, $\Gamma^{(3b)}(E = 2E_{3/2}) = 0.31$ MeV.

Spectroscopic factors $S_n = 1$ can be used in Eq. (3) for the upper limit estimates. This is not a spectroscopic factor for $p_{3/2}$ neutron emission in ${}^8\text{He}$, but a factor $S_n \equiv S_{2n}$ for the two-neutron $[p_{3/2}^2]_0$ configuration in ${}^8\text{He}$. According to estimates (see Eq. (2) in [3]), its value depends on the relative weights of the $[p_{3/2}^4]_0$ and $[p_{3/2}^2 p_{1/2}^2]_0$ configurations in the structure of ${}^8\text{He}$ and is limited from above as $S_{2n} \leq 1$. Width values $\Gamma_3 = 0.59, 0.67, 0.76,$ and 0.85 MeV are obtained for $E^* = 3.6, 3.7, 3.8,$ and 3.9 MeV, respectively.

One can see in the inset to Fig. 4 that at very low energies the 2^+ decay takes place in a «three-body regime», $\sigma \sim E^4$. Above the ${}^7\text{He} + n$ threshold energy, the population probability transfers to the «two-body p -wave regime», $\sigma \sim (E - E_{3/2})^{3/2}$. The cross-section

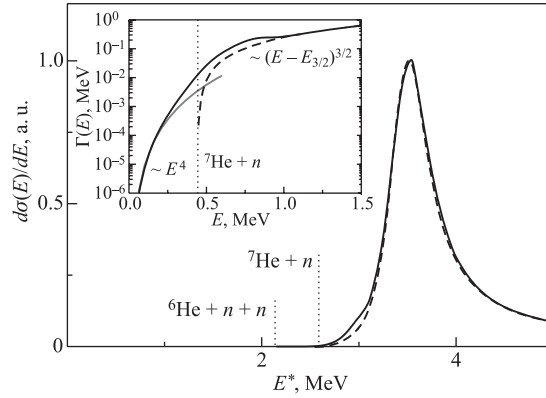


Fig. 4. Profile of the population cross section for the 2^+ state in ${}^8\text{He}$ estimated by Eq.(1). The solid and dashed lines correspond to the width estimated by Eqs. (5) and (4), respectively. The widths as functions of energy are given in the inset. The gray line in the inset is function E^4 illustrating the low-energy behaviour of the three-body sequential width (5)

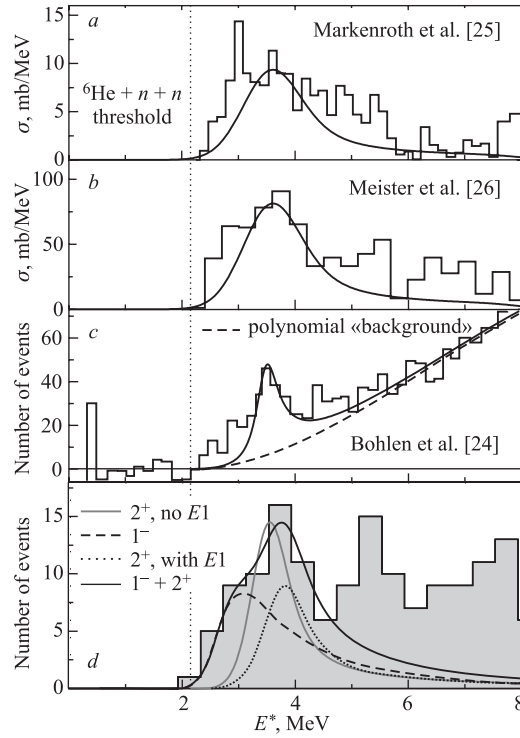


Fig. 5. *a-c*) Experimental spectra from [24–26] are compared to the theoretical profile of the 2^+ state Eq.(1). Panel *d* shows comparison with our data (see Fig.3). Gray curve gives only the 2^+ state contribution, while solid curve represents the fit by both 2^+ and 1^- contributions. The dashed curve is the same as the dashed curve in Fig.6,*d*. Theoretical curves are in each case convoluted with the experimental resolution

profile shows a peculiar behaviour at about $E = 2E_{3/2}$; it is not absolutely clear to which extent this peculiarity is physical and to which it is connected with model assumptions in the derivation of Eq. (5).

The estimated cross-section profile in Fig. 4 demonstrates a small population of the continuum below ~ 0.6 MeV. Figure 5 shows different experimental results compared with the cross-section profile convoluted with the experimental resolution of each experiment. We can see that the low-energy tail of the 2^+ state can hardly be responsible for the near threshold events in either case.

4. POSSIBLE NATURE OF THE THRESHOLD STATE IN ${}^8\text{He}$

The only plausible source of the low-energy events, we have found, is the population of the 1^- continuum. Theoretical studies of such a continuum populated in reactions [10–12] show that the profile of the 1^- cross section typically well resembles the profile of the electromagnetic strength function dB_{E1}/dE . Such functions for spatially extended halo systems could provide very low-energy peak — the so-called soft dipole mode — even without formation of any 1^- resonant state.

We estimate the $E1$ strength function for the ${}^8\text{He} \rightarrow {}^6\text{He} + 2n$ dissociation using the model developed in [20]. The model is based on the usage of a simplified Hamiltonian and is quite schematic. However, it allows one to arrive at important qualitative conclusions, sufficient for our purposes here. The $E1$ strength function is found in that model as

$$\frac{dB_{E1}}{dE} = \frac{2J_f + 1}{2J_i + 1} \frac{X^2}{2\pi} \text{Im} \left[\int d\Omega_x \int d\mathbf{Y} \Psi_E^{(+)\dagger} \frac{\nabla_x}{M_x} \Psi_E^{(+)} \right] \Big|_{X \rightarrow \infty}. \quad (6)$$

Vectors \mathbf{X} and \mathbf{Y} are Jacobi coordinates for the ${}^6\text{He}-n$ and $({}^6\text{He}-n)-n$ subsystems, respectively. The wave function (WF) with outgoing asymptotic

$$\Psi_E^{(+)}(\mathbf{X}, \mathbf{Y}) = \int d\mathbf{X}' d\mathbf{Y}' G_E^{(+)}(\mathbf{X}\mathbf{X}', \mathbf{Y}\mathbf{Y}') \hat{D} \Psi_{E_b}^{(g.s.)}(\mathbf{X}, \mathbf{Y}) \quad (7)$$

is generated by the dipole operator \hat{D} , acting on the g.s. WF $\Psi_{E_b}^{(g.s.)}$. The ground state WFs are constructed for simplicity in the factorized form

$$\Psi_{E_b}^{(g.s.)}(\mathbf{X}, \mathbf{Y}) = \Psi_{E_b/2}^{(x)}(\mathbf{X}) \Psi_{E_b/2}^{(y)}(\mathbf{Y}), \quad (8)$$

where the WFs of the subsystems evenly share the binding energy E_b . The WF of such a form tends to overestimate the radial extent of the WF (which is known to influence the profile of the $E1$ strength function strongly). To compensate for that we somewhat overbind the g.s. WFs in our estimates ($E_b = 1.5$ MeV instead of 0.9 MeV in ${}^6\text{He}$ and $E_b = 2.5$ MeV instead of 2.14 MeV in ${}^8\text{He}$).

Estimating the dipole strength for the light p -shell nuclei we can well take into account only the $[p^2] \rightarrow [sp]$ transitions and neglect the nn interaction and s -wave interaction between the core and neutron (unless the latter is not strongly attractive). In this approximation the three-body Green's function (GF) has a simple analytical form

$$G_E^{(+)}(\mathbf{X}\mathbf{X}', \mathbf{Y}\mathbf{Y}') = \frac{1}{2\pi i} \int dE_{\tau\text{He}} G_{E_{\tau\text{He}}}^{(+)}(\mathbf{X}, \mathbf{X}') G_{E-E_{\tau\text{He}}}^{(+)}(\mathbf{Y}, \mathbf{Y}'),$$

where the two-body GF $G_{E_{7\text{He}}}^{(+)}$ in the X subsystem corresponds to the p -wave continuum with the ${}^7\text{He}$ g.s. $3/2^-$ resonance at $E_{7\text{He}} = 0.445$ MeV. We use in this work the l -dependent Gaussian form factors

$$V_{x,y}^{(l)}(r) = V_{x,y}^{(l)} \exp[-(r/r_0)^2]$$

with radius $r_0 = 2.32$ fm (potentials of this kind were used in [10] for calculations in ${}^6\text{He}$).

The two-body GF $G_{E-E_{7\text{He}}}^{(+)}$ is a free motion GF in the Y subsystem. In principle, the s -wave interaction is known to be repulsive in ${}^5\text{He}$, due to Pauli principle, and is expected to be repulsive in ${}^7\text{He}$. To simulate a possible repulsion effect in the core-neutron s -wave channel we also used in our calculations the repulsive s -wave potential in the Y subsystem. This approximation is justified by the fact that the Jacobi Y coordinate is reasonably close to the core-neutron coordinate r_{cn} , see Fig. 1; in the limit of infinitely heavy core $Y \rightarrow r_{\text{cn}}$. It can be seen in Fig. 6 that repulsion in s wave leads to a significant redistribution of the $E1$ strength to higher energy, but the peak position in the strength function is not influenced noticeably.

Results of the model calculations, including the ${}^6\text{He} \rightarrow nn$ test, are shown in Fig. 6. The estimated ${}^6\text{He}$ strength function giving peak at about 1.1 MeV is in a reasonable agreement with the complete three-body calculations [10] giving peak at about 1.3 MeV (see Fig. 6, *a*). It can be seen that the strength function profile in ${}^6\text{He}$ is sensitive to two main aspects of the dynamics.

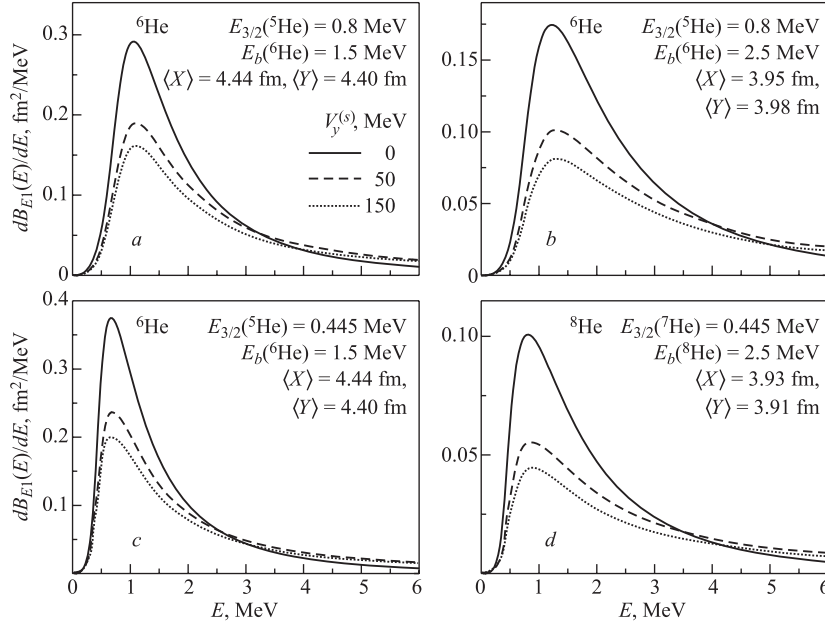


Fig. 6. The $E1$ strength functions for ${}^6\text{He}$ and ${}^8\text{He}$ estimated by Eq.(6). Panels *b* and *c* show calculations made for ${}^6\text{He}$ with unrealistic parameters demonstrating trends in the strength functions behaviour with the parameter variation. $\langle X \rangle$ and $\langle Y \rangle$ are the root mean square X and Y coordinate values for the ground state WFs (8). Solid, dashed and dotted curves correspond to different values of the «unphysical» s -wave potential $V_y^{(s)}$ in the Y subsystem

1. Energy of the resonance ground state in the p -wave subsystem. Figure 6, *c* shows that the strength function peak is shifting to the *lower* energy if the ${}^5\text{He}$ $3/2^-$ state is artificially shifted from the experimental $E_{5\text{He}} = 0.9$ MeV position to the *lower*, 0.445 MeV.

2. «Size» of the ground state WF. Figure 6, *b* shows the strength function peak shifting to *higher* energy if we artificially overbind the ${}^6\text{He}$ g.s. WF to $E_b = 2.5$ MeV, instead of 1.5 MeV, *decreasing* its radial extent. A notion about the radial properties of the g.s. WFs one can have from the root mean square values of the X and Y coordinates indicated in Fig. 6.

When we turn from ${}^6\text{He}$ to ${}^8\text{He}$ (see Fig. 6, *d*) these dynamical trends work in the opposite directions and largely compensate each other (the ${}^8\text{He}$ g.s. is more «compact» than the ${}^6\text{He}$ g.s., but the ${}^7\text{He}$ g.s. resonance is lower than the ${}^5\text{He}$ g.s. resonance). As a result, we find the strength function peak position in ${}^8\text{He}$ to be somewhat lower than the respective position in ${}^6\text{He}$. This indicates that in ${}^8\text{He}$, where the 2^+ state has a significantly higher excitation energy than in ${}^6\text{He}$, the lowest energy feature in the continuum could be the 1^- excitation.

The behaviour of the cross section for the ${}^8\text{He}$ continuum population with the estimated $E1$ component taken into account is shown in Fig. 5, *d*. Without $E1$ contribution the data are in agreement with the standard position ($E \approx 3.6$ MeV) of the 2^+ state, but the near threshold behaviour of the cross section cannot be reproduced. The 2^+ population cross section in this case can be estimated as ~ 250 $\mu\text{b/sr}$. The addition of the 1^- contribution allows one to reproduce the low-energy part of the spectrum much better. In that case we can allow up to 60% feeding to the 1^- continuum. Then we get ~ 100 $\mu\text{b/sr}$ for the 2^+ population and have to shift to about $E \approx 3.9$ MeV the position of this state.

5. DISCUSSION

The proposed significant contribution of the 1^- cross section is not an absolutely unknown phenomenon. Let us discuss the recent experimental data on the ${}^8\text{He}$ 2^+ state.

The experimental data [15] show a sharp rise straight from the ${}^6\text{He} + n + n$ threshold. These data, however, cannot be instructive in that respect due to the insufficient energy resolution (~ 1 MeV). The experimental spectrum from paper [24] is shown in Fig. 5, *c*. Energy resolution in this experiment is high (~ 0.15 MeV) and cannot cause any doubt. Inspected around the ${}^6\text{He} + n + n$ threshold «on a large scale» the spectrum shows the presence of the low-energy intensity which cannot be attributed to the tail of the 2^+ state. Strong population of the $E1$ continuum in ${}^8\text{He}$ in nuclear processes has been demonstrated in a comparison made for the nuclear and Coulomb dissociation data [25, 26]. However, in the interpretation of the data presented in [25, 26] the idea was accepted that the $E1$ cross section in ${}^8\text{He}$ should peak at *higher* energy than in ${}^6\text{He}$ (maximum at about $E \approx 2$ MeV above the threshold). This idea is based on *one* of the two major dynamical aspects of the $E1$ strength function discussed above (namely, the smaller size of ${}^8\text{He}$ compared to ${}^6\text{He}$). Actual situation, as we demonstrate in this work, appears to be more complicated. As a result, the authors of [25, 26] have had to position the 2^+ state *below* the $E1$ peak. Consequently, they had to ascribe to it a very low excitation energy 2.9 MeV (compared to about 3.6 MeV in [15] and in other recent works). The assumption of the very low-energy soft dipole peak in ${}^8\text{He}$ would probably allow one to explain in a more natural way the data from [25, 26]. Also,

there exists a large uncertainty in the definition of the «standard» position of the 2^+ state in ${}^8\text{He}$ (2.7–3.6 MeV, see [2]). We think that a significant component of the disagreement among different experimental works could be connected with the possibility that the 2^+ state is typically observed in a mixture with the 1^- contribution.

The sum rules are important for understanding the $E1$ strength distributions. The cluster NEW sum rule value depends only on the geometric properties of the g.s. WF. For neutron halo nuclei, where only the core has charge (Z_{core}) that sum rule is

$$S_{\text{NEW}} = \frac{3}{4\pi} e^2 Z_{\text{core}}^2 \langle r_{\text{core}}^2 \rangle, \quad (9)$$

where \mathbf{r}_{core} is the core vector in the cms of the nucleus. For ${}^6\text{He}$ our model provides $S_{\text{NEW}} = 1.6 \text{ e}^2 \cdot \text{fm}^2$ which is reasonably close to the result of realistic calculations [10] $S_{\text{NEW}} = 1.37 \text{ e}^2 \cdot \text{fm}^2$. For ${}^8\text{He}$ we have a NEW sum rule value which is not drastically different: $S_{\text{NEW}} = 1.3 \text{ e}^2 \cdot \text{fm}^2$. However, it is easy to see in Fig. 6, *a* and *d* that the $E1$ strength concentrated in the low-energy region is very different in ${}^6\text{He}$ and ${}^8\text{He}$. In our model this feature also strongly depends on the unphysical potential $V_y^{(s)}$. However, it is easy to find that the ratio

$$\frac{S_{\text{NEW}}({}^6\text{He}, E < E_0)}{S_{\text{NEW}}({}^8\text{He}, E < E_0)} \approx 3 \quad (10)$$

is not sensitive to this unphysical parameter. This result is in good agreement with the experimental ratio: $S_{\text{NEW}}({}^6\text{He}, E < 10) = (1.2 \pm 0.2) \text{ e}^2 \cdot \text{fm}^2$ [7], $S_{\text{NEW}}({}^8\text{He}, E < 7) = (0.38 \pm 0.7) \text{ e}^2 \cdot \text{fm}^2$ [26]. Above we have shown that the latter result could have different interpretation in the sense of the $E1$ strength function profile. However, we think that the sum rule value obtained in this work is not very dependent on this problem and is reasonably reliable.

CONCLUSION

In this work we studied the ${}^8\text{He}$ spectrum in the (t, p) transfer reaction. The ground 0^+ and the excited 2^+ ($E^* = 3.6\text{--}3.9$ MeV), (1^+) ($E^* = 5.3\text{--}5.5$ MeV) states of ${}^8\text{He}$ are populated with cross sections 200, $\sim 100\text{--}250$, and $\sim 90\text{--}125 \mu\text{b/sr}$. Some evidence for the third excited state at about $E^* = 7.5$ MeV is obtained. We demonstrate that the near-threshold events observed at about $E \sim 2.14$ MeV cannot be connected with the population of the 2^+ resonance «wing». The estimates of the $E1$ strength function profile in ${}^8\text{He}$ show that the formation of the soft dipole mode in the ${}^8\text{He}$ continuum can be a plausible explanation. The generation of such a mode with a very low peak energy ($E^* \sim 3$ MeV, $E \sim 0.9$ MeV) in nuclear reactions could possibly be an explanation to the controversial results obtained on 2^+ state in the other ${}^8\text{He}$ experiments as well.

The angular correlation measurements in proximity of the ${}^6\text{He} + n + n$ threshold could provide definitive clarification of the 2^+ state problem, e.g., the interference of the 2^+ and 1^- spectra in this energy range could be seen as backward–forward asymmetry in the distribution of the charged ${}^8\text{He}$ decay fragment (${}^6\text{He}$).

Acknowledgements. We are grateful to Profs. B. V. Danilin, S. N. Ershov, and M. V. Zhukov for illuminating discussions. The authors acknowledge the financial support from the Russian RFBR Grant No.08-02-00089. L. V. G. is supported also by the German DFG Grant 436 RUS 113/907/0-1, Russian RFBR Grant 05-02-17535, and Russian Ministry of Industry and Science Grant NS-1885.2003.2.

REFERENCES

1. NNDC database. <http://www.nndc.bnl.gov/nsr>
2. Tilley D. R. et al. // Nucl. Phys. A. 2004. V. 745. P. 155.
3. Golovkov M. S. et al. nucl-ex/0804.0310v1.
4. Kobayashi T. et al. // Phys. Lett. B. 1989. V. 232. P. 51.
5. Arne R. et al. // Phys. Lett. B. 1990. V. 250. P. 19.
6. Blank B. et al. // Z. Phys. A. 1991. Bd. 340. S. 41.
7. Aumann T. et al. // Phys. Rev. C. 1999. V. 59. P. 1252.
8. Palit R. et al. // Phys. Rev. C. 2003. V. 68. P. 034318.
9. Alhassid Y., Gai M., Bertsch G. F. // Phys. Rev. Lett. 1982. V. 49. P. 1482.
10. Danilin B. V. et al. // Nucl. Phys. A. 1998. V. 632. P. 383.
11. Ershov S. N., Danilin B. V., Vaagen J. S. // Phys. Rev. C. 2001. V. 64. P. 054608.
12. Ershov S. N. et al. // Phys. Rev. C. 2004. V. 70. P. 054608.
13. Chulkov L. et al. // Nucl. Phys. A. 2005. V. 759. P. 23.
14. Rodin A. M. et al. // Nucl. Instr. Meth. A. 1997. V. 391. P. 228.
15. Korshennikov A. A. et al. // Phys. Lett. B. 1993. V. 316. P. 38.
16. Tilquin I. et al. // Nucl. Instr. Meth. A. 1995. V. 365. P. 446.
17. Skaza F. et al. // Nucl. Phys. A. 2007. V. 788. P. 260c.
18. Grigorenko L. V., Zhukov M. V. // Phys. Rev. C. 2007. V. 76. P. 014008.
19. Grigorenko L. V., Zhukov M. V. // Ibid. P. 014009.
20. Grigorenko L. V. et al. // Phys. Lett. B. 2006. V. 641. P. 254.
21. Pieper S. C., Wiringa R. B., Carlson J. // Phys. Rev. C. 2004. V. 70. P. 054325.
22. Navrátil P., Ormand W. E. // Phys. Rev. Lett. 2002. V. 88. P. 152502.
23. Volya A., Zelevinsky V. // Phys. Rev. Lett. 2005. V. 94. P. 052501.
24. Bohlen H. G. et al. // Proc. of LEND'95. World Sci., 1995. P. 53.
25. Markenroth K. et al. // Nucl. Phys. A. 2001. V. 679. P. 462.
26. Meister M. et al. // Nucl. Phys. A. 2002. V. 700. P. 3.

Received on June 26, 2008.